Supporting Information

Improving the Activity of Electrocatalysts toward Hydrogen Evolution Reaction, Oxygen Evolution and Reduction Reaction via Modification of Metal and Ligand of Conductive Two-Dimensional Metal-Organic Frameworks

Yanan Zhou,[a,#] Li Sheng,[b,#] Qiquan Luo,[c,*] Wenhua Zhang,[d,*] and Jinlong Yang[a,*]

a Hefei National Laboratory for Physical Sciences at the Microscale, CAS Key Laboratory of Materials for Energy Conversion and Synergetic Innovation Centre of Quantum Information and Quantum Physics, University of Science and Technology of China, Hefei, Anhui 230026, China

b Department of Chemical Physics, University of Science and Technology of China, Hefei, Anhui 230026, China

c Institutes of Physical Science and Information Technology, Anhui University, Hefei 230601, China

d Key Laboratory of Materials for Energy Conversion, Chinese Academy of Sciences (CAS), Department of Materials Science and Engineering, University of Science and Technology of China, Hefei, Anhui, 230026, China

[#]Yanan Zhou and Li Sheng contributed equally to this work.

*Email: jlyang@ustc.edu.cn; whhzhang@ustc.edu.cn; qluo@ustc.edu.cn.

1. Computational methods

All calculations were performed by using the Vienna a*b initio* Simulation Package (VASP)[1,2] based on the density functional theory. The projector augmented wave (PAW) method was used to describe the ion-electron interactions.[3] The generalized gradient approximation (GGA)[4] with the Perdew-Burke-Ernzerhof (PBE)[5] functional was used to describe the electronic exchange-correlation interactions. The Van der Waals (vdW) effect was described by using Grimme's DFT-D3 correction method.[6] The cutoff energy was set to 500 eV for the plane-wave basis set. The convergence criterion for energy and force during

geometrical optimization was set to 10^{-5} eV and 10^{-2} eV/Å, respectively. The Brillouin zone was sampled with a 3 x 3 x 1 Monkhorst-Pack mesh grid[7] during optimization. The vacuum space of 20 Å was used to avoid the interlayer interaction in the *z* direction. The solvent effect was considered by using the implicit solvent model as implemented in VASPsol with the dielectric constant of 78.4 for water.[8] Ab initio molecular dynamics (AIMD) simulations was performed to examine dynamical stability of the designed catalyst, and the algorithm of the Nose thermostat was carried out to simulate a canonical ensemble[9] for 10 ps with a time step of 2 fs. Bader charge analysis was performed to investigate the charge transfer process.[10] The calculation details for the HER, OER and ORR under acidic condition are listed in the followings content.

The formation energy (E_f) and dissolution potential (U_{diss}) are defined as the following equations:

$$E_f = (E_{total} - E_{substrate} - 3E_{TM})/3 \quad (1)$$

$$U_{diss} = U_{diss}^{\circ}\,(bulk) - E_f/ne \quad (2)$$

Where, E_{total} and $E_{substrate}$ are the total energies of TMN_xO_{4-x}-HTP system and N_xO_{4-x}-HTP substrate, respectively. E_{TM} is the total energy of a metal atom in its most stable bulk structure. U_{diss}° (bulk) is the standard dissolution potential of bulk metal, *n* is the number of electrons involved during the dissolution process. Since E_{TM} is referenced with respect to its bulk metal, systems with negative values of E_f are evaluated to be thermodynamically stable against the clustering of TM atoms. Systems with positive values of U_{diss} vs standard hydrogen electrode (SHE) are considered to be electrochemically stable.

The descriptor φ involving the TM site and its nearest neighboring N/O atoms was calculated as following:

$$\varphi = \theta_d \times \frac{\chi_{aver}}{\chi_O} \quad (3)$$

Here, θ_d refers to the valance electron number of the TM atom, χ_{aver} refers to the average electronegativity of the TM atom and its nearest neighboring N/O atoms, and χ_O refers to the electronegativity of the O atom. χ_{aver} is defined as $(\chi_{TM} + n\chi_{N/O})/(n + 1)$, where χ_{TM} and $\chi_{N/O}$ refers to the electronegativities of the TM and N/O atoms, respectively, and *n* is the number of N/O atoms (in this work, *n* is 4).

2. HER

Under the standard conditions of U = 0 and pH = 0, the whole HER process can be described by the following equation (4):

$$H^+ (aq) + e^- \rightarrow 1/2\ H_2\ (g) \qquad (4)$$

The overall HER reaction mechanism includes a three-state diagram, that is, an initial state $H^+ (aq) + e^-$, an intermediate adsorbed H* and the final product 1/2 H_2 (g). The total energy of $H^+ (aq) + e^-$ is equal to that of 1/2 H_2 (g) under the standard electrode voltage condition.[11] To evaluate the HER catalytic activity of one catalyst, the difference Gibbs free energy of adsorbed hydrogen (ΔG_{H^*}) was calculated by using the following equation (5) as a key descriptor for the HER activity[12]:

$$\Delta G_{H^*} = \Delta E_{H^*} + \Delta E_{ZPE} - T\Delta S_{H^*} \qquad (5)$$

Here, ΔE_{H^*} refers to the adsorption energy of hydrogen and defined as $\Delta E_{H^*}=E_{catalyst+H^*}-E_{catalyst}-1/2E_{H2,g}$, $E_{catalyst+H^*}$ refers to the total energy of the hydrogen adsorbed on the catalyst, $E_{catalyst}$ is the total energy of the clean catalyst without hydrogen adsorbed, and E_{H2} is the energy of a hydrogen molecule in the gas phase. ΔE_{ZPE} is the difference in zero-point energy between the adsorbed hydrogen and hydrogen in the gas phase. ΔS_{H^*} is the entropy difference between the adsorbed state and the gas phase of hydrogen. The values of ΔE_{ZPE} and ΔS_{H^*} can be obtained from the vibration frequency calculations of the system. ΔE_{ZPE} can be calculated by $\Delta E_{ZPE} = E_{ZPE}(H^*) - 1/2E_{ZPE}(H_2)$, obtained from the vibrational frequencies calculation for the adsorbed hydrogen. The contributions to ΔS_{H^*} are small, thus, can be neglected. The ZPE and the entropy of the adsorbed adsorbents have the close values even on different systems.

3. OER and ORR

The overall OER process includes a four-stage pathway, which can be described as follows in the acidic environment:

$$2H_2O \rightarrow 4H^+ + O_2 + 4e- \qquad (6)$$

The four electron reaction paths of OER are defined as equations (a) - (d) as reported in the previous literature[13]:

$$H_2O\ (l) + * \rightarrow HO* + H^+ + e- \qquad (a)$$

$$HO* \rightarrow O* + H^+ + e- \qquad (b)$$

$$O* + H_2O\ (l) \rightarrow HOO* + H^+ + e- \qquad (c)$$

$$HOO* \rightarrow * + O_2\ (g) + H^+ + e- \qquad (d)$$

Where * represents active sites on the catalyst, (*l*) and (g) is the liquid and gas phase, respectively, and O*, HO* and HOO* are the corresponding adsorbed intermediates. The Gibbs free energy (ΔG) of each elementary step under the U = 0 and pH = 0 condition was calculated by the following equations (6a~6d):

$$\Delta G_a = G_{HO*} + 1/2 G_{H2,g} - G_{H2O,l} - G_* \quad (6a)$$

$$\Delta G_b = G_{O*} + 1/2 G_{H2,g} - G_{HO*} \quad (6b)$$

$$\Delta G_c = G_{HOO*} + 1/2 G_{H2,g} - G_{O*} - G_{H2O,l} \quad (6c)$$

$$\Delta G_d = \{4.92eV + 2G_{H2O,l} - 2G_{H2,g}\} + 1/2 G_{H2,g} + G_* - G_{HOO*} \quad (6d)$$

Where we defined $G_{X*}=E_{X*}+ZPE_{X*}-TS_{X*}$, X refers to HO*, O* and HOO*. Here E_{X*} is the DFT total energy of the corresponding X* system under the polarization solvent model calculation. ZPE_{X*} refers to the zero-point energy of X*. Here we only include the zero-point energy of X*, while keeping the catalyst * fixed. TS_{X*} is the calculated entropy term of the adsorbed intermediate. Finally, $G_*=E_*$ is the total energy of catalyst under the DFT solvent model calculation. Due to the poor description of DFT for the high-spin ground state of the O_2, we used $G_{O2,g} + 4G_{H2,g} - 2G_{H2O,l} = 4.92$ eV to obtain the free energy of O_2 in the gas phase.[14] It is also difficult to directly calculate the Gibbs free energy of H_2O in the liquid phase ($G_{H2O,l}$). It is customary to calculate the liquid phase Gibbs free energy from its vapor phase counterpart at their equilibrium pressure when they have the same Gibbs free energies. Then, $G_{H2O,l} = E_{H2O} + ZPE_{H2O} - TS_{H2O}$. Where, E_{H2O} is total energy of H_2O in the gas phase obtained from the DFT calculation; ZPE_{H2O} is the zero point energy; TS_{H2O} is the entropy term of the gas phase (in equilibrium with the liquid phase). We took the values of 0.67 eV and 0.41 eV for the TS_{H2O} and TS_{H2}, respectively.[15] The free energy changes for the above four OER processes can be described as $\Delta G_a = \Delta G_{HO*}$, $\Delta G_b = \Delta G_{O*} - \Delta G_{HO*}$, $\Delta G_c = \Delta G_{HOO*} - \Delta G_{O*}$, and $\Delta G_d = 4.92 - \Delta G_{HOO*}$. As the most important measure of the catalytic activities for OER, overpotential η of OER (η^{OER}) was calculated by equation (7):

$$\eta^{OER} = \frac{\max\{\Delta G_a, \Delta G_b, \Delta G_c, \Delta G_d\}}{e} - 1.23 \quad (7)$$

ORR, as a reverse reaction of the OER, its overpotential (η^{ORR}) can be calculated by the following equation (8):

$$\eta^{ORR} = 1.23 - \frac{\min\{\Delta G_a, \Delta G_b, \Delta G_c, \Delta G_d\}}{e} \quad (8)$$

While, because HER, OER and ORR occur under different electric potentials, thus there

is no competitive selectivity among them. In detail, as shown in **Figure S1a**, for the water splitting system, when the applied positive potential is larger than 1.23 V, the corresponding OER can take place at the anode of the cell; when the applied negative potential is lower than 0, the HER can take place at the cathode side of cell. For the metal-air battery, the ORR can take place when the applied positive potential range is from 0 to 1.23 V, while the OER can take place when the applied positive potential is larger than 1.23 V.

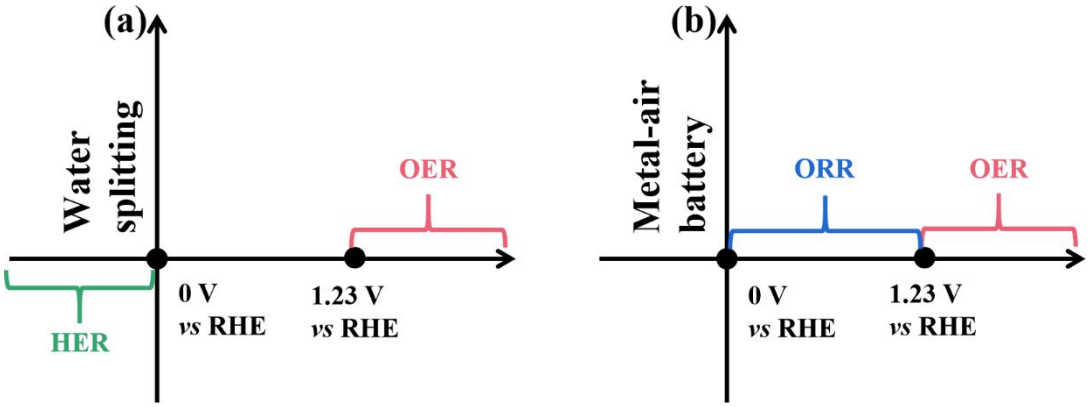

Figure S1 Schematic diagrams show the work potential range of (a) HER and OER for electrocatalytic water splitting, and (b) ORR and OER for metal-air batteries. The two equilibrium points, 0 and 1.23 V *vs*. reversible hydrogen electrode (RHE) are the equilibrium potential for the hydrogen- and oxygen-based electrocatalytic reactions.

4. The polarization curves simulation of OER and ORR

For a given electrochemical process O + *ne* ⇌ R under one electric potential *U*, it can be used the well-known Nerst equation to link the concentrations of the reactant and the product[16] by the following equation (9):

$$U = U_0 + \frac{RT}{nF}\ln\left(\frac{C_O}{C_R}\right) \qquad (9)$$

Here, U_0 refers to the equilibrium potential of the reaction at the standard state, *R* refers to the universal gas constant, *T* refers to the temperature, *n* refers to the electron transfer number, F refers to the Faraday constant, and C_O/C_R refers to the concentration of the reactant/product in this reaction.[17] Therefore, the exchange current density j_0 can be calculated by the following equation (10):

$$j_0 = nFkC_O\exp\left[-\frac{\alpha F}{RT}(U_{eq} - U_0)\right] = nFkC_O^{1-\alpha}C_R^{\alpha} \qquad (10)$$

Where k refers to the reaction rate constant, U_{eq} refers to the equilibrium potential, and α refers to the transfer coefficient. So, the electrochemical polarization equation can be defined by equation (11):

$$j = j_0\left[\exp\left(-\frac{\alpha F}{RT}\eta\right) - \exp\left(\frac{(1-\alpha)F}{RT}\eta\right)\right] \quad (11)$$

Where $\eta = U - U_{eq}$ refers to the overpotential deviated from the equilibrium potential and j of the overall current density. The exchange current density j_0 can be used to evaluate the catalytic activity of one catalyst. Following the electrochemical catalysis mode developed by Nørskov,[13] the reaction rate constant k can be defined as follows:

$$k = k_0 exp\left[-\frac{\Delta G_{max}}{k_b T}\right] \quad (12)$$

Where k_b and ΔG_{max} refers to the Boltzmann constant and the Gibbs free energy change of the potential-determining step, respectively. In the electrochemical polarization model,[18] k_0 is defined as the equation (13):

$$k_0 = \frac{k_b T}{h} \quad (13)$$

Where h refers to the Planck constant. Therefore, the exchange current density j_0 of the electrochemical reaction when the reaction approaches its equilibrium state can be described as the following equation (14):

$$j_0 = nFC_O\frac{k_b T}{h}exp\left[-\frac{\Delta G_{max}}{k_b T}\right] \quad (14)$$

Hence, the overall current density j can be calculated by the follows equation (15) according to the overpotential η[18]:

$$j = nFC_O\frac{k_b T}{h}exp\left[-\frac{\Delta G_{max}}{k_b T}\right]\left[\exp\left(-\frac{\alpha F}{RT}\eta\right) - \exp\left(\frac{(1-\alpha)F}{RT}\eta\right)\right] \approx nFC_O\frac{k_b T}{h}exp\left[-\frac{\Delta G_{max}}{k_b T} - \frac{\alpha F}{RT}\eta\right]$$

(15)

The OER and ORR need to overcome the reaction kinetic energy barriers, and the onset potential generally represents the reaction potential at which the current begins to deviate from the baseline.[19] In this work, the calculated polarization curves for the OER and ORR was calculated as literature reported.[20]

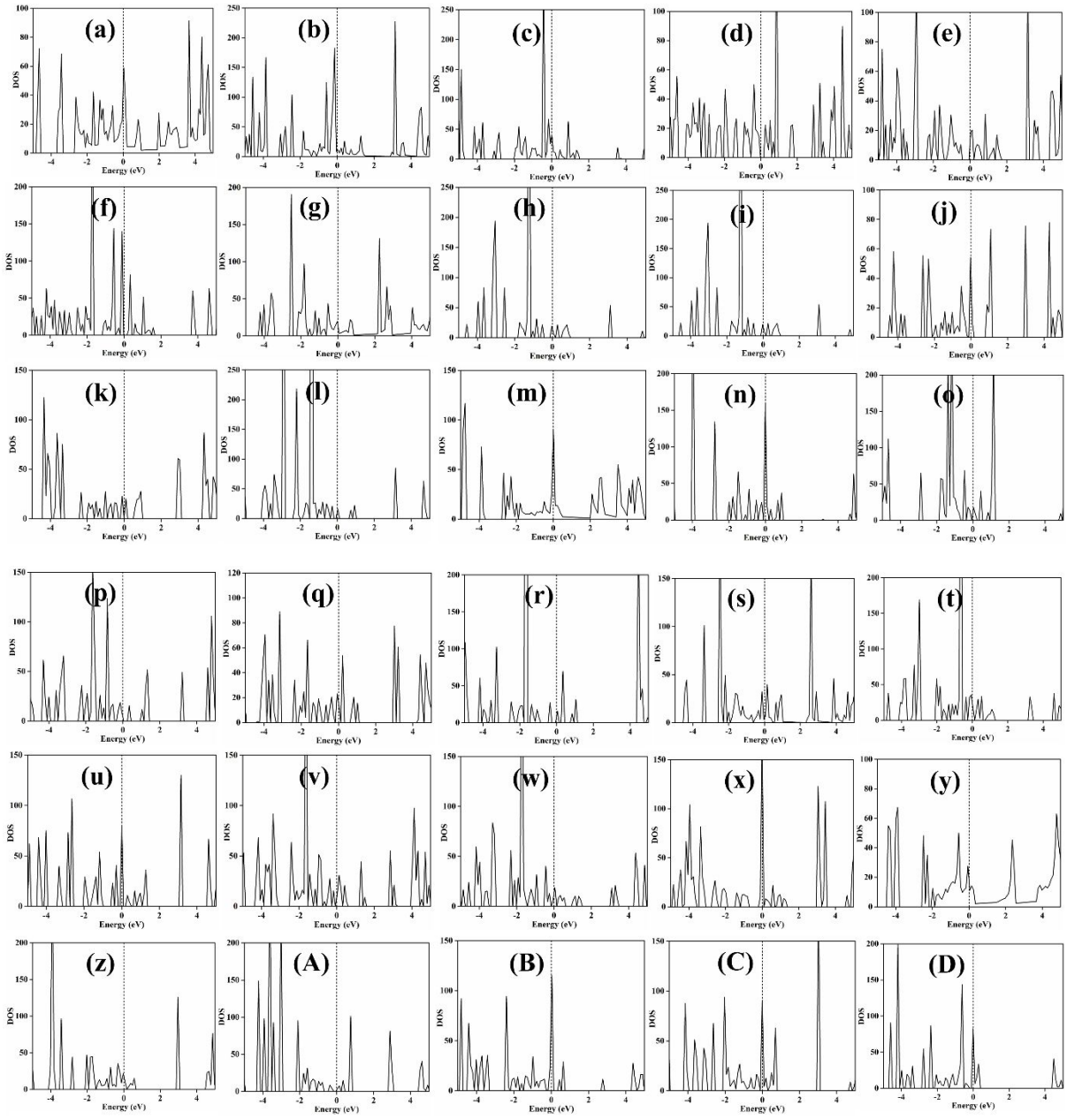

Figure S2 Calculated density of states (DOS) for (a) FeN_4-HTP, (b) CoN_4-HTP, (c) NiN_4-HTP, (d) RuN_4-HTP, (e) RhN_4-HTP, (f) PdN_4-HTP, (g) FeN_1O_3-HTP, (h) CoN_1O_3-HTP, (i) NiN_1O_3-HTP, (j) RuN_1O_3-HTP, (k) RhN_1O_3-HTP, (l) PdN_1O_3-HTP, (m) FeN_2O_2-HTP, (n) CoN_2O_2-HTP, (o) NiN_2O_2-HTP, (p) RuN_2O_2-HTP, (q) RhN_2O_2-HTP, (r) PdN_2O_2-HTP, (s) FeN_3O_1-HTP, (t) CoN_3O_1-HTP, (u) NiN_3O_1-HTP, (v) RuN_3O_1-HTP, (w) RhN_3O_1-HTP, (x) PdN_3O_1-HTP, (y) FeO_4-HTP, (z) CoO_4-HTP, (A) NiO_4-HTP, (B) RuO_4-HTP, (C) RhO_4-HTP, and (D) PdO_4-HTP. The Fermi level is set at the zero of energy (dashed line in figures).

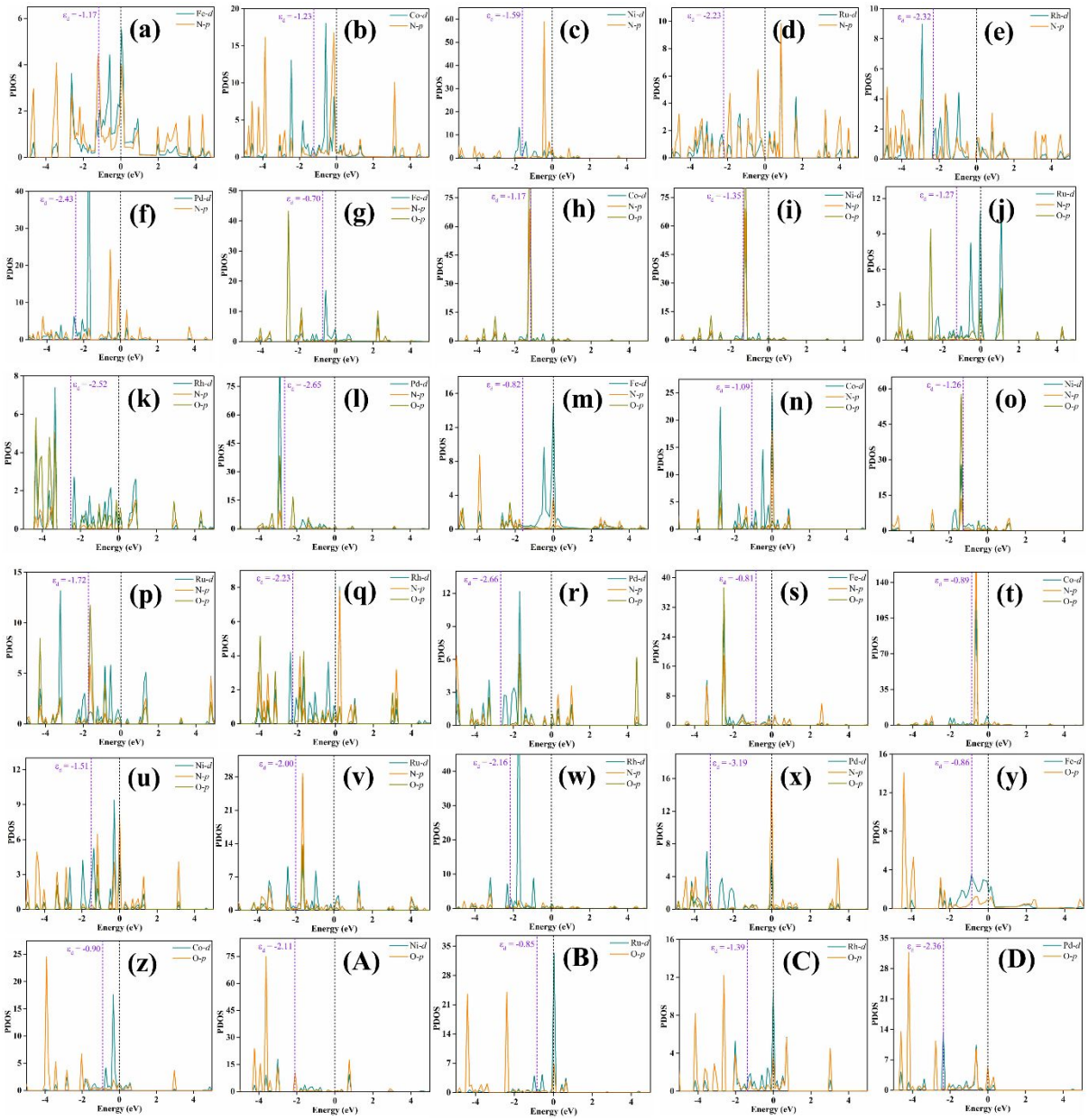

Figure S3 Calculated partial density of states (PDOS) for the *d* orbital of TM and *p* orbital of N/O atoms for (a) FeN_4-HTP, (b) CoN_4-HTP, (c) NiN_4-HTP, (d) RuN_4-HTP, (e) RhN_4-HTP, (f) PdN_4-HTP, (g) FeN_1O_3-HTP, (h) CoN_1O_3-HTP, (i) NiN_1O_3-HTP, (j) RuN_1O_3-HTP, (k) RhN_1O_3-HTP, (l) PdN_1O_3-HTP, (m) FeN_2O_2-HTP, (n) CoN_2O_2-HTP, (o) NiN_2O_2-HTP, (p) RuN_2O_2-HTP, (q) RhN_2O_2-HTP, (r) PdN_2O_2-HTP, (s) FeN_3O_1-HTP, (t) CoN_3O_1-HTP, (u) NiN_3O_1-HTP, (v) RuN_3O_1-HTP, (w) RhN_3O_1-HTP, (x) PdN_3O_1-HTP, (y) FeO_4-HTP, (z) CoO_4-HTP, (A) NiO_4-HTP, (B) RuO_4-HTP, (C) RhO_4-HTP, and (D) PdO_4-HTP. The Fermi level is set at the zero of energy (dashed line in figures).

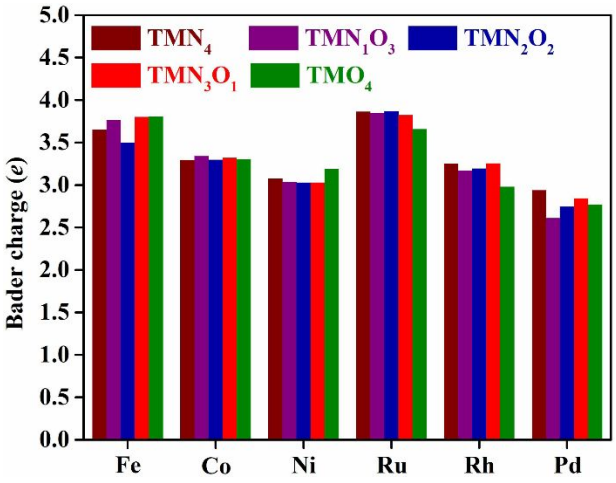

Figure S4 Calculated charge transfer from TM atoms to N_xO_{4-x} substrates of TMN_xO_{4-x}-HTP obtained by Bader charge analysis. The positive value of Bader charge suggests that the charge is transferred from TM atoms to the substrates.

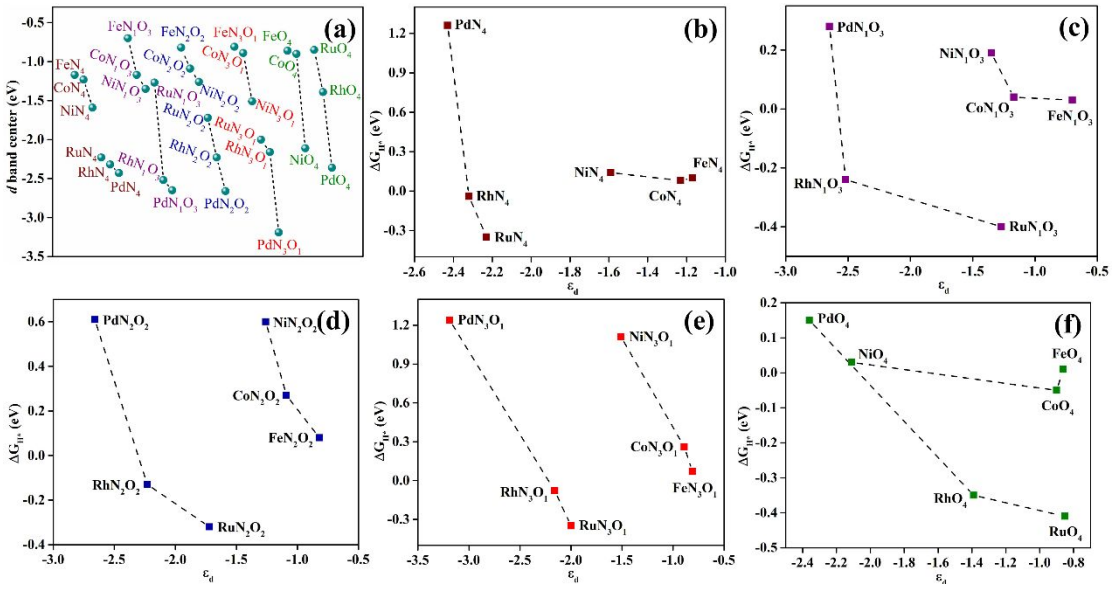

Figure S5 (a) calculated *d*-band center (ε_d) for all the TMN_xO_{4-x}-HTP systems. Calculated ΔG_{H^*} values corresponding to the *d*-band center ε_d for (b) TMN_4-HTP, (c) TMN_1O_3-HTP, (d) TMN_2O_2-HTP, (e) TMN_3O_1-HTP, and (f) TMO_4-HTP systems.

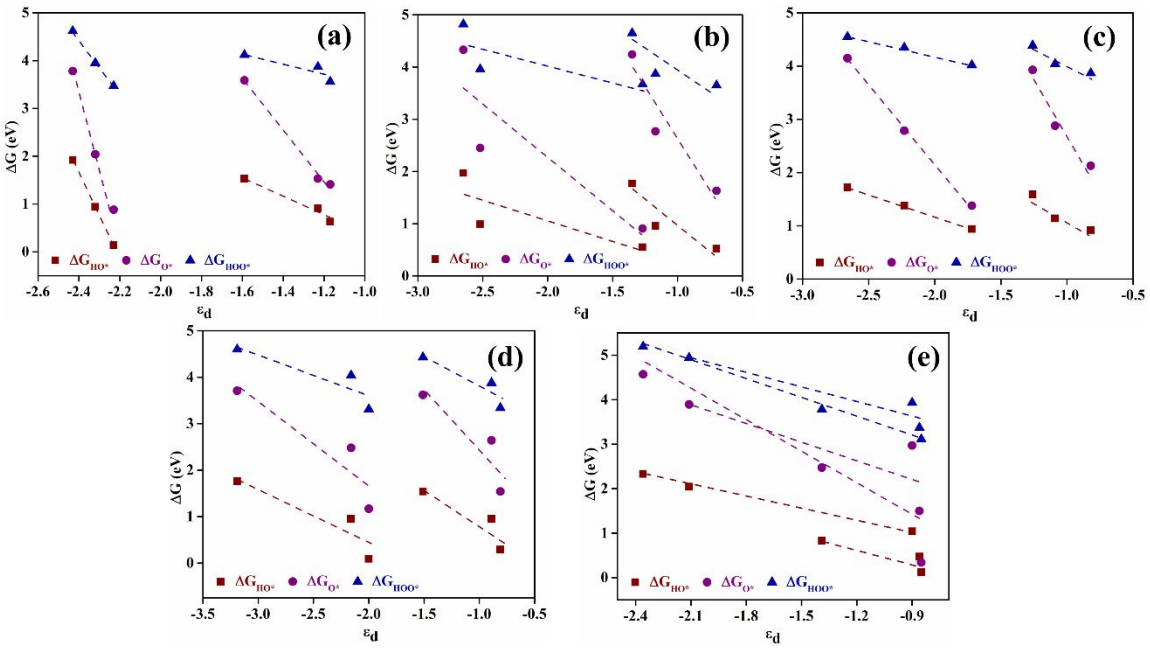

Figure S6 Gibbs free energy of intermediates corresponding to the *d*-band center ε_d for (a) TMN_4-HTP, (b) TMN_1O_3-HTP, (c) TMN_2O_2-HTP, (d) TMN_3O_1-HTP, and (e) TMO_4-HTP systems.

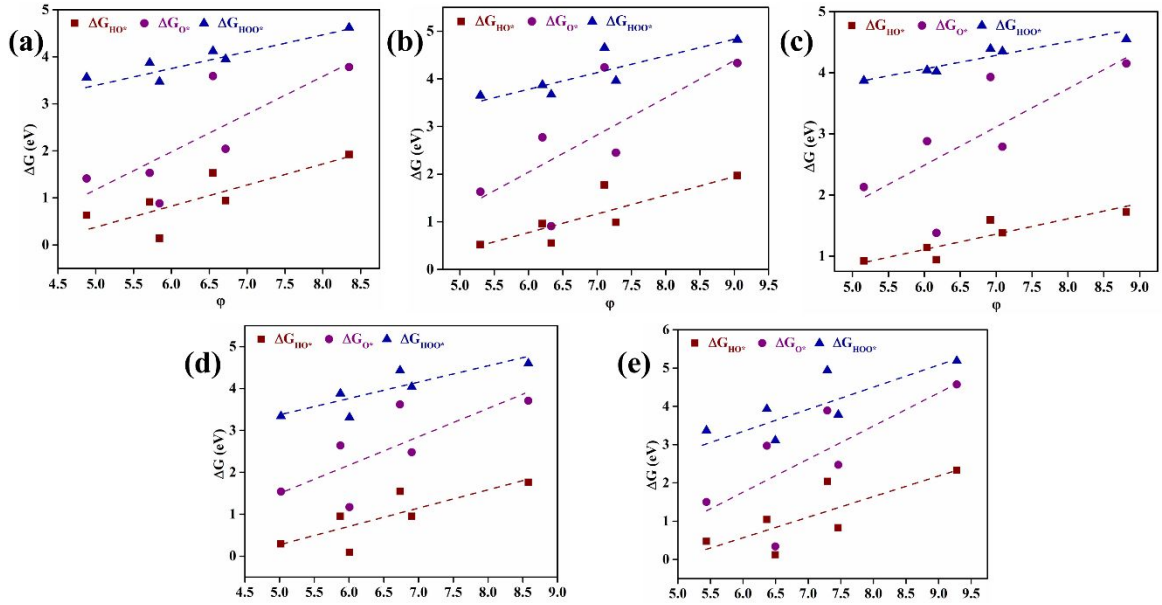

Figure S7 Gibbs free energy of HO*, O*, and HOO* versus the descriptor φ for (a) TMN_4-HTP, (b) TMN_1O_3-HTP, (c) TMN_2O_2-HTP, (d) TMN_3O_1-HTP, and (e) TMO_4-HTP systems.

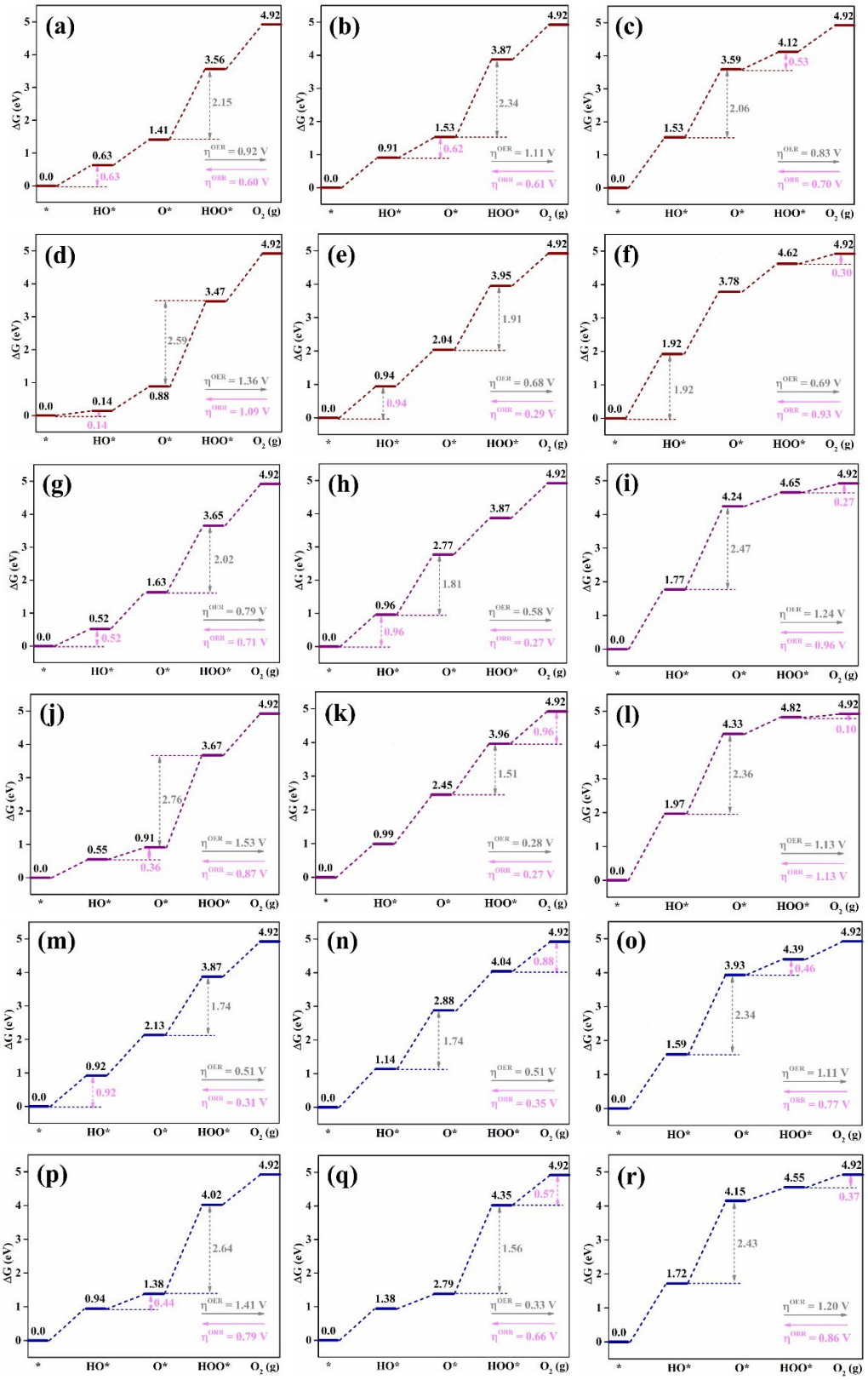
(a)
0.0
0.63
1.41
3.56
4.92
0.63
2.15
η^OER = 0.92 V
η^ORR = 0.60 V
(b)
0.0
0.91
1.53
3.87
4.92
0.62
2.34
η^OER = 1.11 V
η^ORR = 0.61 V
(c)
0.0
1.53
3.59
4.12
4.92
0.53
2.06
η^OER = 0.83 V
η^ORR = 0.70 V
(d)
0.0
0.14
0.88
3.47
4.92
0.14
2.59
η^OER = 1.36 V
η^ORR = 1.09 V
(e)
0.0
0.94
2.04
3.95
4.92
0.94
1.91
η^OER = 0.68 V
η^ORR = 0.29 V
(f)
0.0
1.92
3.78
4.62
4.92
1.92
0.30
η^OER = 0.69 V
η^ORR = 0.93 V
(g)
0.0
0.52
1.63
3.65
4.92
0.52
2.02
η^OER = 0.79 V
η^ORR = 0.71 V
(h)
0.0
0.96
2.77
3.87
4.92
0.96
1.81
η^OER = 0.58 V
η^ORR = 0.27 V
(i)
0.0
1.77
4.24
4.65
4.92
2.47
0.27
η^OER = 1.24 V
η^ORR = 0.96 V
(j)
0.0
0.55
0.91
3.67
4.92
0.36
2.76
η^OER = 1.53 V
η^ORR = 0.87 V
(k)
0.0
0.99
2.45
3.96
4.92
0.96
1.51
η^OER = 0.28 V
η^ORR = 0.27 V
(l)
0.0
1.97
4.33
4.82
4.92
2.36
0.10
η^OER = 1.13 V
η^ORR = 1.13 V
(m)
0.0
0.92
2.13
3.87
4.92
0.92
1.74
η^OER = 0.51 V
η^ORR = 0.31 V
(n)
0.0
1.14
2.88
4.04
4.92
0.88
1.74
η^OER = 0.51 V
η^ORR = 0.35 V
(o)
0.0
1.59
3.93
4.39
4.92
0.46
2.34
η^OER = 1.11 V
η^ORR = 0.77 V
(p)
0.0
0.94
1.38
4.02
4.92
0.44
2.64
η^OER = 1.41 V
η^ORR = 0.79 V
(q)
0.0
1.38
2.79
4.35
4.92
0.57
1.56
η^OER = 0.33 V
η^ORR = 0.66 V
(r)
0.0
1.72
4.15
4.55
4.92
0.37
2.43
η^OER = 1.20 V
η^ORR = 0.86 V
ΔG (eV)
*
HO*
O*
HOO*
O2 (g)

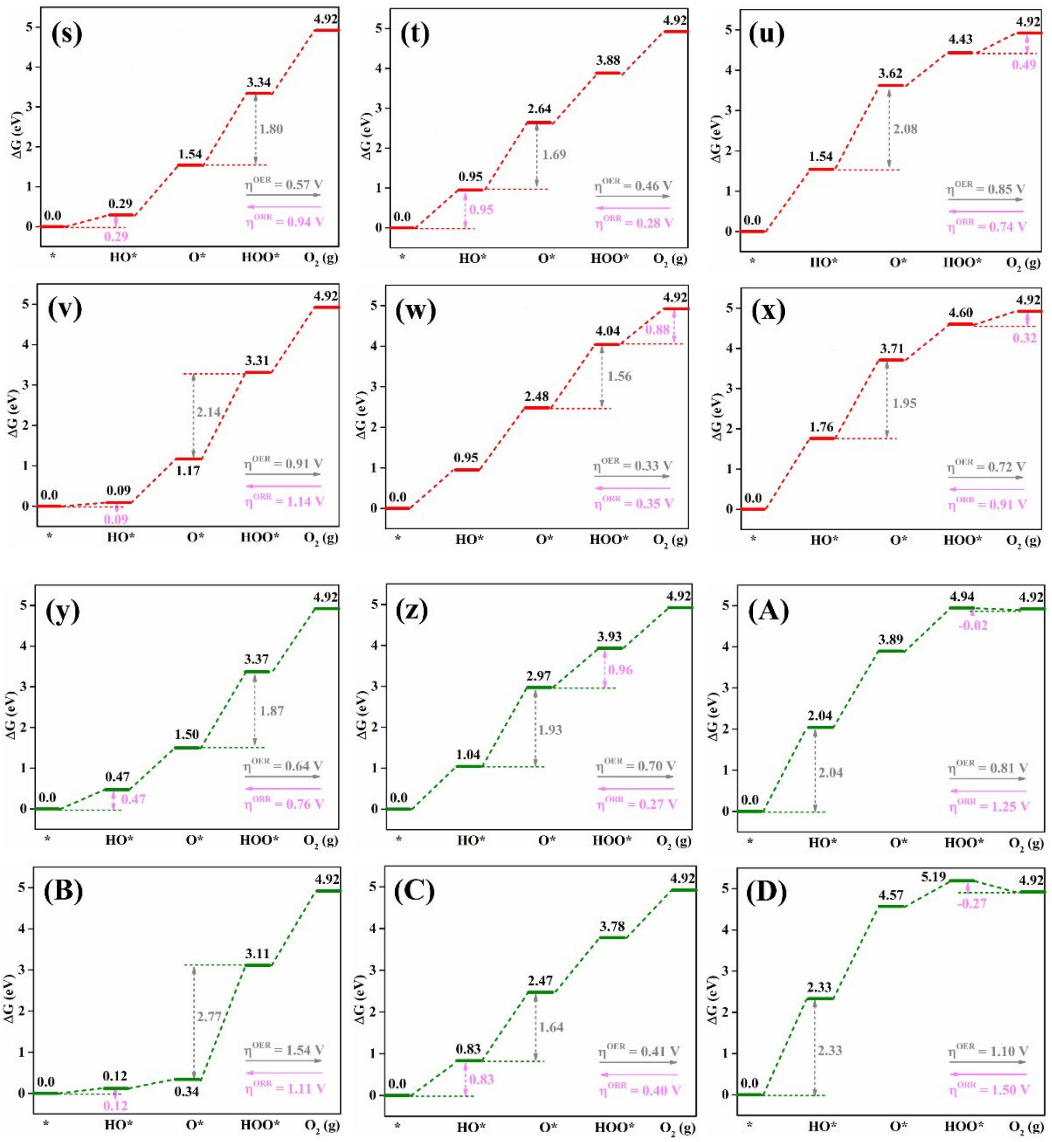

Figure S8 Calculated free energy diagrams of OER and ORR on (a) FeN_4-HTP, (b) CoN_4-HTP, (c) NiN_4-HTP, (d) RuN_4-HTP, (e) RhN_4-HTP, (f) PdN_4-HTP, (g) FeN_1O_3-HTP, (h) CoN_1O_3-HTP, (i) NiN_1O_3-HTP, (j) RuN_1O_3-HTP, (k) RhN_1O_3-HTP, (l) PdN_1O_3-HTP, (m) FeN_2O_2-HTP, (n) CoN_2O_2-HTP, (o) NiN_2O_2-HTP, (p) RuN_2O_2-HTP, (q) RhN_2O_2-HTP, (r) PdN_2O_2-HTP, (s) FeN_3O_1-HTP, (t) CoN_3O_1-HTP, (u) NiN_3O_1-HTP, (v) RuN_3O_1-HTP, (w) RhN_3O_1-HTP, (x) PdN_3O_1-HTP, (y) FeO_4-HTP, (z) CoO_4-HTP, (A) NiO_4-HTP, (B) RuO_4-HTP, (C) RhO_4-HTP, and (D) PdO_4-HTP at zero potential. The grey and pink values are the rate-limiting step values for OER and ORR.

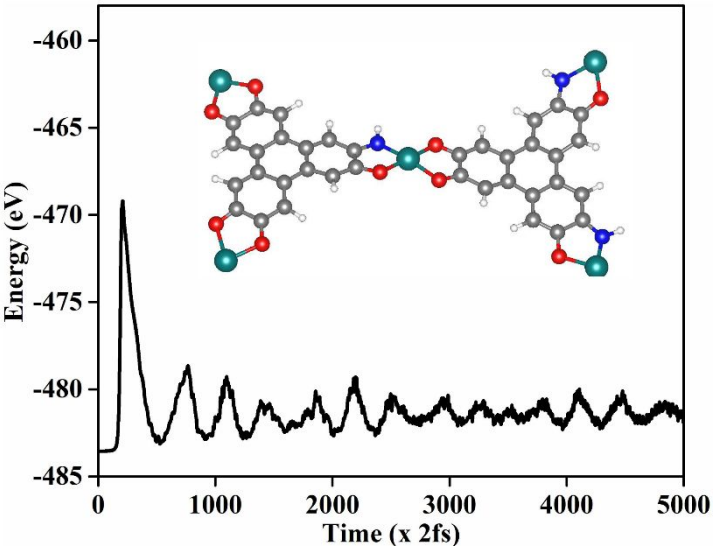

Figure S9 Total energy variations of RhN_1O_3-HTP as the function of time for AIMD simulation, and the snapshot of atomic configuration at the end of the AIMD simulation is inserted.

Table S1 Calculated ΔG_{H^*} values for different systems, and the unit of ΔG_{H^*} is eV.

System	ΔG_{H^*}	System	ΔG_{H^*}	System	ΔG_{H^*}	System	ΔG_{H^*}	System	ΔG_{H^*}
FeN_4	0.10	FeN_1O_3	0.03	FeN_2O_2	0.08	FeN_3O_1	0.07	FeO_4	0.01
CoN_4	0.08	CoN_1O_3	0.04	CoN_2O_2	0.27	CoN_3O_1	0.26	CoO_4	-0.05
NiN_4	0.14	NiN_1O_3	0.19	NiN_2O_2	0.60	NiN_3O_1	1.11	NiO_4	0.03
RuN_4	-0.35	RuN_1O_3	-0.40	RuN_2O_2	-0.32	RuN_3O_1	-0.35	RuO_4	-0.41
RhN_4	-0.04	RhN_1O_3	-0.24	RhN_2O_2	-0.13	RhN_3O_1	-0.08	RhO_4	-0.35
PdN_4	1.26	PdN_1O_3	0.28	PdN_2O_2	0.61	PdN_3O_1	1.24	PdO_4	0.15

REFERENCES

(1) Kresse G.; Furthmuller, J. Efficiency of Ab-Initio Total Energy Calculations for Metals and Semiconductors Using A Plane-Wave Basis Set. *Comput. Mater. Sci*. **1996**, *6*, 15-50.
(2) Kresse G.; Furthmuller, J. Efficient iterative schemes for ab initio total-energy calculations using a plane-wave basis set. *Phys. Rev. B: Condens. Matter Mater. Phys*. **1996**, *54*, 11169-11186.
(3) Blochl, P. E. Projector Augmented-Wave Method. *Phys. Rev. B: Condens. Matter Mater. Phys*. **1994**, *50*, 17953-17979.
(4) Perdew, J. P.; Burke, K.; Ernzerhof, M. Generalized Gradient Approximation Made Simple. *Phys. Rev. Lett*. **1996**, *77*, 3865-3868.

(5) Perdew, J. P.; Ernzerhof, M.; Burke, K. Rationale for Mixing Exact Exchange with Density Functional Approximations. *J. Chem. Phys*. **1996**, *105*, 9982-9985.
(6) Grimme, S.; Antony, J.; Ehrlich, S.; Krieg, H. A Consistent and Accurate Ab Initio Parametrization of Density Functional Dispersion Correction (DFT-D) for the 94 Elements H-Pu *J. Chem. Phys*. 2010, **132**, 154104-154123.
(7) Monkhorst, H. J.; Pack, J. D. Special Points for Brillouin-Zone Integrations. *Phys. Rev. B: Condens. Matter Mater. Phys*. 1976, **13**, 5188-5192.
(8) Mathew, K.; Sundararaman, R.; Letchworth-Weaver, K.; Arias, T. A.; Hennig, R. G. Implicit Solvation Model for Density-Functional Study of Nanocrystal Surfaces and Reaction Pathways. *J. Chem. Phys*. **2014**, *140*, 084106-084114.
(9) Martyna, G. J.; Klein, M. L.; Tuckerman, M. Nosé–Hoover Chains: The Canonical Ensemble via Continuous Dynamics. *J. Chem. Phys*. **1992**, *97*, 2635-2643.
(10) Tang, W.; Sanville, E.; Henkelman, G. A. Grid-Based Bader Analysis Algorithm Without Lattice Bias. *J. Phys. Condens. Matter*. **2009**, *21*, 084204.
(11) Gao, G. P.; Bottle S.; Du, A. J. Understanding the Activity and Selectivity of Single Atom Catalysts for Hydrogen and Oxygen Evolution via Ab Initial Study. *Catal. Sci. Technol.* **2018**, *8*, 996-1001.
(12) Hinnemann, B.; Moses, P. G.; Bonde, J.; Jørgensen, K. P.; Nielsen, J. H.; Horch, S.; Chorkendorff, I.; Nørskov, J. K. Biomimetic Hydrogen Evolution: MoS_2 Nanoparticles as Catalyst for Hydrogen Evolution. *J. Am. Chem. Soc*. **2005**, *127*, 5308-5308.
(13) Nørskov, J. K.; Rossmeisl, J.; Logadottir, A.; Lindqvist, L. Origin of the Overpotential for Oxygen Reduction at A Fuel-Cell Cathode. *J. Phys. Chem. B*. **2004**, *108*, 17886-17892.
(14) Valdes, A.; Qu, Z. W.; Kroes, G. J. Oxidation and Photo-Oxidation of Water on TiO_2 Surface. *J. Phys. Chem. C*. **2008**, *112*, 9872-9879.
(15) Atkins, P.; Paula, J. Atkins' Physical Chemistry, Oxford University Press, **2014**.
(16) Feiner, A. S.; McEvoy, A. J. The Nernst Equation. *J. Chem. Educ*. **1994**, *71*, 493.
(17) Jiao, Y.; Zheng, Y.; Jaroniec, M.; Qiao, S. Z. Design of Electrocatalysts for Oxygen-and Hydrogen-Involving Energy Conversion Reactions. *Chem. Soc. Rev*. **2015**, *44*, 2060.
(18) Ma, H.; Chen, X. Q.; Li, R. H.; Wang, S. L.; Dong, J. H.; Ke, W. First-Principles Modeling of Anisotropic Anodic Dissolution of Metals and Alloys in Corrosive Environments. *Acta Mater*. **2017**, *130*, 137.
(19) Huang, Z.; Wang, J.; Peng, Y.; Jung, C.; Fisher, A.; Wang, X. Design of Efficient Bifunctional Oxygen Reduction/Evolution Electrocatalyst: Recent Advances and Perspectives. *Adv. Energy Mater*. **2017**, *7*, 1700544.
(20) Wei, B.; Fu, Z. H.; Legut, D.; Germann, T. C.; Du, S. Y.; Zhang, H. J.; Francisco, J. S.; Zhang, R. F. Rational Design of Highly Stable and Active MXene-Based Bifunctional ORR/OER Double-Atom Catalysts. *Adv. Mater*. **2021**, 2102595.